PLOS Climate

RESEARCH ARTICLE

Bias correction with a deep neural model to improve Global Climate Model salinity projections in the Bay of Bengal

Abhishek Pasula[1], **Deepak N. Subramani**[1,2*]

1 Department of Computational and Data Sciences, Indian Institute of Science, Bengaluru, India,
2 Divecha Center for Climate Change, Indian Institute of Science, Bengaluru, India

* deepakns@iisc.ac.in

Citation: Pasula A, Subramani DN (2026) Bias correction with a deep neural model to improve Global Climate Model salinity projections in the Bay of Bengal. PLOS Clim 5(3): e0000749. https://doi.org/10.1371/journal.pclm.0000749

Editor: Ahmed Kenawy, Mansoura University, EGYPT

Received: September 22, 2025

Accepted: February 14, 2026

Published: March 19, 2026

Data availability statement: All code and data produced in this work are available on GitHub (https://github.com/AbhiPasula/CNRM-CM6-Salinity-Bias-Correction.git).

Funding: The compute used in this work was supported by the Ministry of Earth Sciences,

Abstract

Global Climate Models (GCMs) simulate the Earth's climate dynamics and forecast the future climate under different shared socioeconomic pathways. However, GCM salinity projections in the Bay of Bengal have high errors as evaluated for the years in which both projections and reanalysis are available. We develop a convolutional encoder-decoder deep neural operator model (UNet) for bias correction of GCM salinity projections in the Bay of Bengal. We analyze the corrected projections quantitatively and qualitatively to examine the mean and variability of surface salinity and the top 200m depth-averaged salinity projections. The root mean square error (RMSE) and Pattern Correlation Coefficient (PCC) analysis quantitatively demonstrate UNet's superior performance compared to the baseline Equi-Distant Cumulative Distribution Function (EDCDF) method for bias correction. The UNet-corrected projections demonstrate significant improvements with up to 45% lower RMSE and 5% higher PCC for sea surface salinity, and up to 35% lower RMSE and 2% higher PCC for 200m depth-averaged salinity during the test period. Crucially, the modified salinity patterns in the UNet-corrected projections suggest changes to major features such as the barrier layer, East India Coastal Current, and Southwest Monsoon Current, which in turn affect the health of mangroves and the primary productivity of the region.

1 Introduction

Climate change represents one of the most significant challenges of our era. Considering the ocean's vital role in climate dynamics, enhancing our understanding of ocean variability and change is essential. Major challenges in understanding the climate system include accurately quantifying the Earth's heat and freshwater balances, with the oceans playing a critical role in both. Climate change affects water circulation and sea surface salinity [1]. Salinity is a crucial physical property of seawater that

Government of India (Reachout Grant MoES/36/OOIS/Extra/84/2022 to DNS).

Competing interests: The authors have declared that no competing interests exist.

influences ocean dynamics by regulating density, stratification, and circulation [2,3]. Salinity quantifies the intensity of the ocean hydrological cycle and plays a vital role in ocean-atmosphere interactions [4]. Thus, capturing changes in salinity accurately is crucial for improved climate projections and global climate change policy-making.

The Indian Ocean is a unique tropical basin that is largely closed off to the north, with restricted connections to other oceans. Its salinity is mainly affected by monsoon rainfall. In the northern Indian Ocean, the Arabian Sea is characterized by high salinity, whereas the Bay of Bengal is known for its lower salinity. The Bay of Bengal is the largest and most stratified bay globally [5,6]. Salinity in the Bay of Bengal is mainly influenced by the influx of freshwater from precipitation and rivers, as well as the remote influx of high-saline water. The Southwest Monsoon Current (SMC), an eastward flowing current in the Indian Ocean near Sri Lanka that supplies salt water to the Bay of Bengal from the Arabian Sea [7–9]. SMC is a surface phenomenon with an intense flow in the top 200 m [7,10]. Our recent research elucidates a significant correlation between salinity variations within the Andaman Sea and the SMC [11]. These studies highlight the essential role salinity plays in the sustainability of marine biodiversity, emphasizing the need to explore the impacts of climate change on salinity to assess potential changes in ocean biodiversity. Although sea surface temperature, sea level, and greenhouse gases are well-established indicators of climate change, the impact of variations in freshwater/seawater salinity has not been thoroughly investigated. Salinity plays a crucial role in the climate system [12], and accurate salinity forecasts are vital to comprehend future changes in the dynamics of global oceans, including the Bay of Bengal.

Global Climate Models (GCMs) such as the Centre National de Recherches M´et´eorologiques Climate Model (CNRM-CM6) are sophisticated computational tools that simulate the Earth's climate dynamics. The Coupled Model Intercomparison Project (CMIP), under the aegis of the World Climate Research Program (WCRP), within the Intergovernmental Panel for Climate Change (IPCC) framework, contains a suite of climate models to project future climate scenarios. Phase 6 (CMIP6) models employ Shared Socioeconomic Pathways (SSP) to simulate the climate impact of possible future global trends [14,15]. These models provide future atmospheric and oceanic projections. However, a significant limitation of GCMs lies in their susceptibility to bias, which could significantly influence decision-making and policy processes. For example, the salinity projections for the Bay of Bengal in the CMIP6 suite have a root mean square error (RMSE) of 4.2 psu (for the CNRM-CM6 SSP1) compared to data from the Ocean Reanalysis System (ORAS5).

Fig 1 illustrates the JJAS (monsoon season) climatology of the top 200 m salinity average (S200mavg) in the Bay of Bengal. Notably, the CNRM-CM6 projections and the ORAS5 reanalysis capture the SMC's signature: high saline water entering the Bay of Bengal from the southwest. However, CNRM-CM6 consistently exhibits both higher salinity values and a different spatial extent of this high salinity in the Bay of Bengal compared to ORAS5. A robust data-driven bias correction is necessary to accurately capture this feature and study its interannual salinity variability in a changing climate.

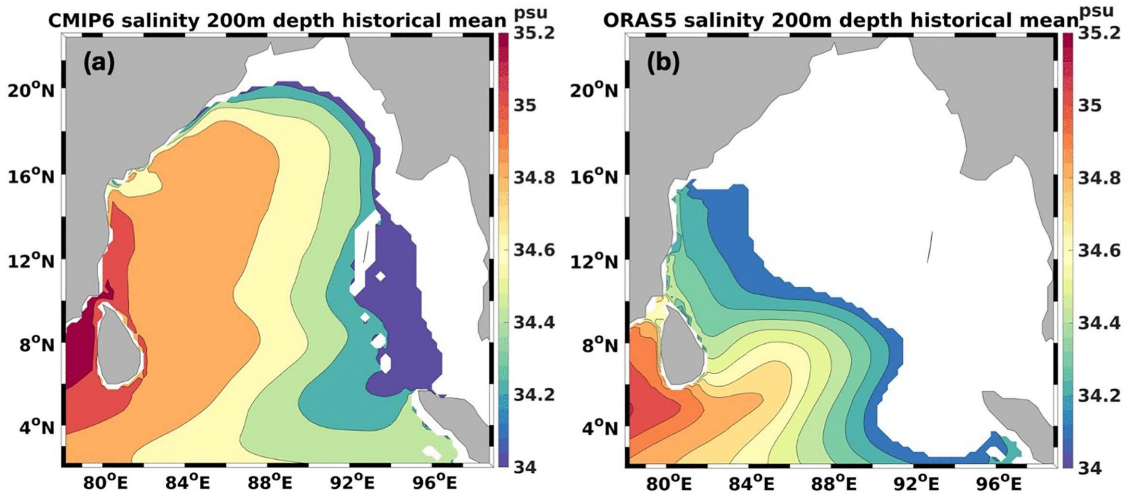

Fig 1. Study Domain. Bay of Bengal domain from 2◦N to 22.5◦N latitude and 78◦E to 99◦E longitude. JJAS climatology for the Bay of Bengal from 1958 to 2014 using **(a)** historical data from the CNRM-CM6 model from CMIP6 and **(b)** ORAS5 reanalysis, show that climate models poorly represent salinity in the Bay of Bengal. Coastline is extracted from NOAA's ETOPO [13].

https://doi.org/10.1371/journal.pclm.0000749.g001

Bias correction approaches for GCM projections can be categorized into statistical or dynamical downscaling, and machine learning methods. Within the statistical framework, bias correction techniques for CMIP ocean models are primarily divided into univariate and multivariate approaches [16–19]. Univariate methods address individual variables independently using interpolation techniques that adjust statistical moments such as mean and variance based on projection and observational datasets. Several prominent univariate techniques have emerged: the delta change approach maintains observational dynamics while generating future time series [20], linear scaling modifies monthly means while preserving observational variability [20], and distribution mapping adjusts model distribution functions to align with observational data [21]. Among these approaches, quantile mapping has gained widespread adoption for correcting distributional properties [16], with the Equi-Distant Cumulative Distribution Function (EDCDF) method emerging as the most popular quantile mapping variant for CMIP6 bias correction applications [22]. Multivariate methods extend beyond individual variable corrections to address inter-variable dependencies and cross-correlations. Notable multivariate techniques include conditional binning, which implements two-dimensional corrections for temperature-precipitation relationships through -based binning followed by quantile mapping [17], and iterative approaches that cyclically apply univariate quantile mapping combined with multivariate corrections across multiple temporal scales [23,24].

Machine learning algorithms enable data-driven predictions through supervised learning, mapping input-output relationships for environmental applications [14]. ML techniques analyze complex ocean-atmospheric data including temperature, precipitation, salinity, and currents to improve understanding of climate dynamics and improve forecast accuracy [25,26]. Deep neural networks, particularly convolutional and transformer models, effectively address spatio-temporal problems [27,28]. Recent applications include bias correction for temperature [29], precipitation [30], wind energy [31], and Indian regional climate variables [32,33]. However, CMIP6 ocean forecast bias correction for the Bay of Bengal using deep learning remains unexplored, presenting significant potential for ML-based climate model improvement. Recently, multiple deep neural network architectures have been explored for GCM bias correction through an extensive ablation study to arrive at the UNet convolutional encoder-decoder neural operator architecture [34]. Bias correctors based on the above architecture have been used to improve the projections of temperature and sea level [35]. However, salinity bias correction using deep models has not been reported in the literature. Building on the aforementioned progress, the purpose of the present

paper is to train a new deep neural model for bias correction of salinity projections in the Bay of Bengal and to apply the trained model to study the dynamical implications of the corrected salinity projections.

2 Materials and methods

To correct the GCM salinity projections of the Bay of Bengal, we employ a UNet Neural Model trained on climatology-removed historical (1958-2014) and projection (2015-2020) data from CMIP6 (CNRM-CM6) as input, with climatology-removed ORAS5
(1958–2020) as ground truth. In what follows, we describe the neural model architecture, detail the datasets used for model development and evaluation, and explain the baseline correction method used for comparative assessment.

2.1 UNet neural model for bias correction of GCM salinity projections

The UNet neural network architecture for salinity bias correction is shown in Fig 2.

A detailed ablation study on this neural operator is described in our recent work [34]. This architecture was selected for its ability to combine global context with local high-resolution features, making it particularly effective for our application, where fine details are as important as the overall structure. A similar architecture was used for the corrections of sea surface temperature and dynamical sea level in the Bay of Bengal [35]. The present paper focuses on using a similar architecture to train new models for correcting SSS and S200mavg projections. We develop and provide data processing utilities alongside a UNet neural network to correct biases in CNRM-CM6 sea surface salinity (SSS) and top 200 m depth-averaged salinity (S200mavg), with our code available on GitHub (https://github.com/AbhiPasula/CNRM-CM6-Salinity-Bias-Correction) [36]. The new set of hyperparameters are also detailed in Section 2.2.

2.2 Training data and procedure

For developing the deep learning data-driven bias correction model based on deep learning for future projections, we selected the Global Climate Model (GCM) CNRM-CM6–1-HR, part of the CMIP6 suite, from the National Center for Meteorological Research (CNRM), France. This model was chosen because it exhibits smaller biases in ocean temperature and salinity compared to previous versions [37], and its projections for ocean heat uptake closely match observed data [38]. The data set includes historical simulations from 1850 to 2014 and extends future projections to 2100 through four shared socioeconomic pathways (SSPs), namely SSP1-2.6, SSP2-4.5, SSP3-7.0, and SSP5-8.5. These scenarios encompass different paths for energy consumption, land use, and emissions, giving different sets of projections based on the scenarios. The CNRM-CM6–1-HR uses a 25 km ocean grid and a 50 km atmospheric grid, allowing complete modeling of the general circulation of the ocean and atmosphere [37].

We selected Ocean Reanalysis System 5 (ORAS5), developed by the European Center for Medium-Range Weather Forecasts (ECMWF), as the reference dataset for training our salinity bias correction model. ORAS5 is configured with the NEMO ocean model version 3.4.1 [39] at a 25 km horizontal resolution and incorporates multiple observational datasets through a 3D-Var assimilation scheme with a 5-day cycle. The system assimilates sea surface temperature, subsurface temperature, salinity profiles, satellite sea level measurements, and sea ice concentration data. ORAS5 nudges the sea surface salinity to climatology [40]. By training the model to minimize error relative to ORAS5, the corrected projections inherently inherit the reanalysis product's systemic biases. Consequently, the corrected salinity represents the best estimate consistent with the ORAS5 reanalysis state rather than absolute observational truth; however, given the paucity of long-term, high-resolution continuous salinity observations in the Bay of Bengal, aligning with the ORAS5 standard represents the current state-of-the-art for minimizing GCM bias. More details about the CNRM and ORAS5 models are provided in the Table A in S1 Text. The same data sources were used for the bias corrections of CNRM-CM6 sea surface temperature in the Bay of Bengal [34].

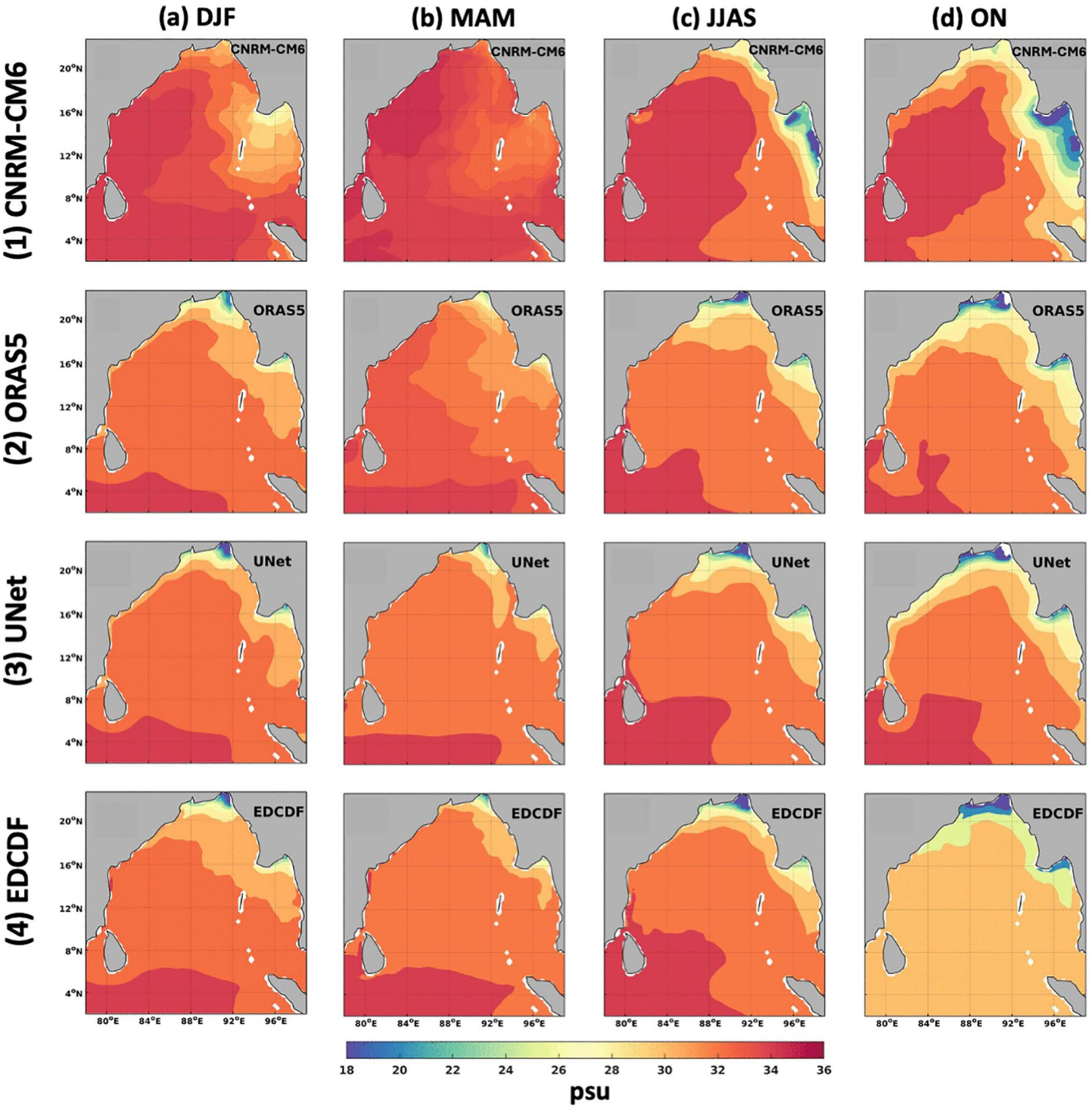

Fig 2. UNet architecture. Input is a 128 × 128 image of the monthly anomaly of GCM salinity projection. The encoder path has five downsampling stages, each with two convolutional layers (3 × 3 filters, tanh activation, and dropout) and one 2 × 2 max pooling. The number of filters doubles at each stage (32, 64, 128, 256, 512), with 1024 channels in the bottleneck layer. The decoder has five upsampling stages, each with one transposed convolution (2 × 2) and two convolutional layers (3 × 3 filters, tanh activation, and dropout). Each stage also combines the upsampled features with the corresponding encoder features through skip connections (a concatenation operation). A 1 × 1 convolutional layer is used to obtain the final output. Coastline in input and output images are extracted from NOAA's ETOPO [13].

https://doi.org/10.1371/journal.pclm.0000749.g002

The selected study region is the Bay of Bengal, which spans from 2◦N to 23◦N latitude and 78◦E to 99◦E longitude, with grid dimensions of 85 × 85 at CNRM and ORAS5 resolution. Historical data span from 1958 to 2014, and projections extend from 2015 to 2100. For training and validation, we used data from 1958 to 2020 (972 months), dividing it into 768 months for training and 204 for cross-validation and hyperparameter selection. The test data are from 2021 to June 2024 (42 months) and are not used in model tuning to avoid data leakage. The use of this short span for testing is dictated by data availability as the ORAS5 reanalysis product is only available up to the present day. The period where both the future projections and reliable reanalysis data overlap is intrinsically limited to the last decade, and this data must be used for deep learning model development and testing purposes. Our underlying assumption is that the systematic bias structure learned from over 60 years of historical data (1958–2020) remains sufficiently stable to be applied to future projections.

Hyperparameters. To select the hyperparameters we performed cross validation using the 204 months in the validation set. A systematic hyperparameter sweep was conducted to fix learning rate, number of encoder-decoder blocks and filter sizes. We initialized weights using the He normal distribution and trained the network with the Adam optimizer. The architecture employs tanh activation functions within the convolutional layers to effectively process the positive and negative anomalies inherent in climate data. To mitigate overfitting, a common challenge due to the high spatial and temporal correlation of climate projections, we integrated dropout layers (0.2) between the encoder and decoder blocks.

The monthly climatology is derived from the ORAS5 data from the training period (1958–2020) and is subtracted from the input and target datasets, aiding the model in correcting the anomalies. Our ablation study indicates that the anomaly correction produces optimal results. All monthly data for GCM and ORAS5 were converted to the input size of 128 × 128 using bilinear interpolation so that the input data dimensions are in a power-of-2 to allow the use of symmetric encoder-decoder structure without padding. Although SSP projections vary, we solely used ORAS5 as the ground truth for all scenarios.

2.3 Complete workflow

Fig 3 illustrates the complete workflow for developing and applying our deep neural operator for salinity bias correction. CNRM-CM6 historical and future projections salinity data (1958–2020) are split into training and validation sets to develop a UNet encoder-decoder architecture (Fig 2). The Mean Squared Error (MSE) guides model optimization, with the best-performing configuration selected based on validation metrics. Once trained, our model is applied during inference to obtain bias-corrected salinity fields corresponding to the future CNRM-CM6 projections (2021–2100).

2.4 EDCDF statistical method for baseline

Quantile mapping is a prevalent interpolation-based bias correction technique that adjusts the distributional properties of the model to more closely match those of historical observations [16]. The most prominent quantile mapping method for climate model bias correction, called the Equi-Distant Cumulative Distribution Function (EDCDF), is used as a baseline to compare the performance of our UNet for bias correction [22]. The EDCDF method corrects the climate projections by comparing the model output with historical observations [22], and employing the resulting CDFs to correct the bias in future projections. Comprehensive validation studies have shown that the EDCDF method reduces biases in GCM projections [41–43], making it an ideal baseline to assess the performance of our neural bias correction approach.

3 Results

The convolutional encoder-decoder neural operator (UNet) models are first trained for bias correction of sea surface salinity (SSS) and top 200 m depth-averaged salinity (S200mavg) projections by CNRM-CM6 in the Bay of Bengal. The trained model is then used to correct the bias in the CNRM-CM6 salinity projections from 2021 to 2100. For the years between 2021 and 2024, the ocean reanalysis data (ORAS5) are accessible, allowing us to use this time frame to assess

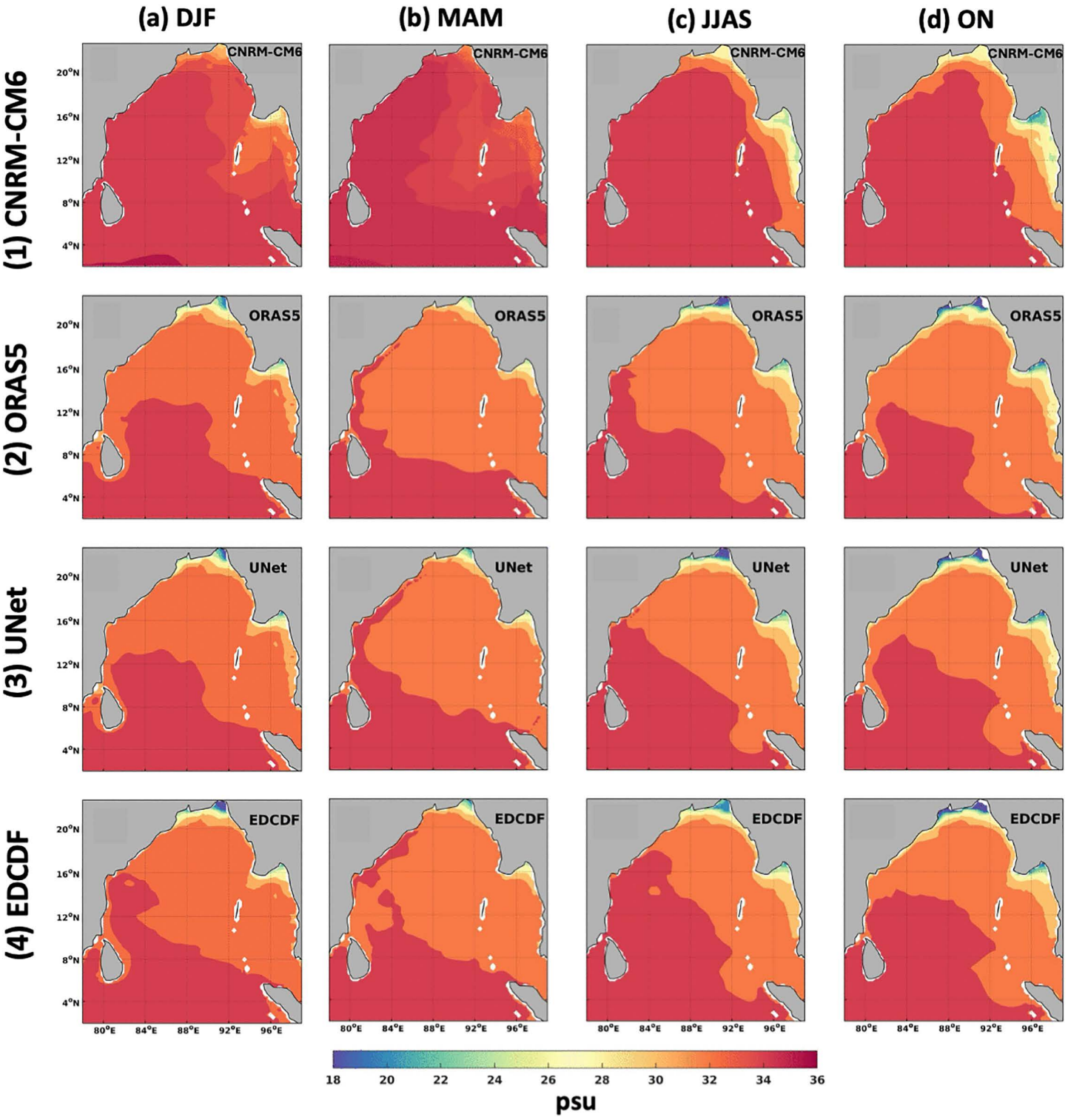

Fig 3. Workflow. Flowchart of the methodological framework for our deep neural operator bias correction model to improve salinity projections in the Bay of Bengal.

https://doi.org/10.1371/journal.pclm.0000749.g003

the efficacy of our UNet model. Subsequently, we study the properties of the corrected salinity projections to understand the dynamical implications of the corrected projections in representing important features in the Bay of Bengal.

3.1 Quantitative evaluation of the salinity bias correction in the test period (2021-2024)

We begin by evaluating the error of our correction model in the test years 2021–2024. Table 1 provides the root mean square error (RMSE) and the pattern correlation coefficient (PCC) of the salinity projections (raw/corrected) compared to the ORAS5 reanalysis. RMSE and PCC are calculated monthly and averaged over the months in the test years. The results for correction with the statistical Equi-Distant Cumulative Distribution Function (EDCDF) correction method (Section 2.4) are also provided. The UNet correction has lower RMSE values for SSS, ranging from 0.52 to 0.61 psu, than the EDCDF correction, which exceeds 0.85 psu. For S200mavg, the UNet-corrected projection outperforms, with RMSE values below 0.28 psu in all SSP scenarios (SSP-1, 2, 3, and 5). In comparison, the uncorrected CNRM-CM6 projections have a very high RMSE between 4.15 and 4.3 psu. More than RMSE, the pattern correlation coefficient captures the similarity in spatial patterns. We see that for both SSS and S200mavg, the PCC is higher for the UNet-corrected projection than the EDCDF, each higher than the uncorrected CNRM-CM6 projections. We performed a paired t-test on the monthly Mean Squared Error (MSE), which revealed that the UNet correction resulted in a statistically significant reduction ($t = 2.7, p < 0.01$; see Figure B-C in S1 Text).

3.2 Comparison of seasonal salinity projections in the test period

The mean Sea Surface Salinity (SSS) and top 200 m depth-averaged salinity (S200mavg) show characteristic north-south gradients across the Bay of Bengal, which vary seasonally. For SSS, the winter season (Fig 4(a) (DJF)) in ORAS5 reanalysis reveals fresher conditions (18–24 psu) in the northern regions, which transitions to higher salinity (30–34 psu) in the southern region. Similarly, S200mavg shows moderate salinity

(28–32 psu) in the north and higher values (32–34 psu) in the south (Fig 5(a) (DJF)). This pattern reflects the persistent influence of freshwater stratification from the northeast monsoon in the north, while the southern region is influenced by the interaction with the equatorial Indian Ocean and the Arabian Sea. The uncorrected CNRM-CM6 model overestimates

Table 1. Performance Metrics: Root Mean Square Error (RMSE) and Pattern.

SSS						
	CNRM		**EDCDF**		**UNet**	
SSP	**RMSE**	**PCC**	**RMSE**	**PCC**	**RMSE**	**PCC**
1	4.2132	0.5882	0.9585	0.8912	0.5217	0.9361
2	4.501	0.5714	0.8622	0.8987	0.6145	0.9248
3	4.1694	0.5679	0.8475	0.8951	0.6112	0.9251
5	4.3043	0.5673	0.7823	0.8973	0.5484	0.9313
S200mavg						
	CNRM		**EDCDF**		**UNet**	
SSP	**RMSE**	**PCC**	**RMSE**	**PCC**	**RMSE**	**PCC**
1	2.1254	0.7542	0.3872	0.9397	0.2519	0.9518
2	2.0524	0.7302	0.3720	0.9435	0.2798	0.9569
3	2.1293	0.7369	0.3532	0.9442	0.2673	0.9585
5	2.0030	0.7285	0.3822	0.9410	0.2610	0.9586

Correlation Coefficient (PCC) of CNRM-CM6, EDCDF corrected, and UNet corrected (a) Sea Surface Salinity (SSS) and (b) 200 m depth-averaged salinity (S200mavg) projections, evaluated against ORAS5 reanalysis in test years 2021–2024.

https://doi.org/10.1371/journal.pclm.0000749.t001

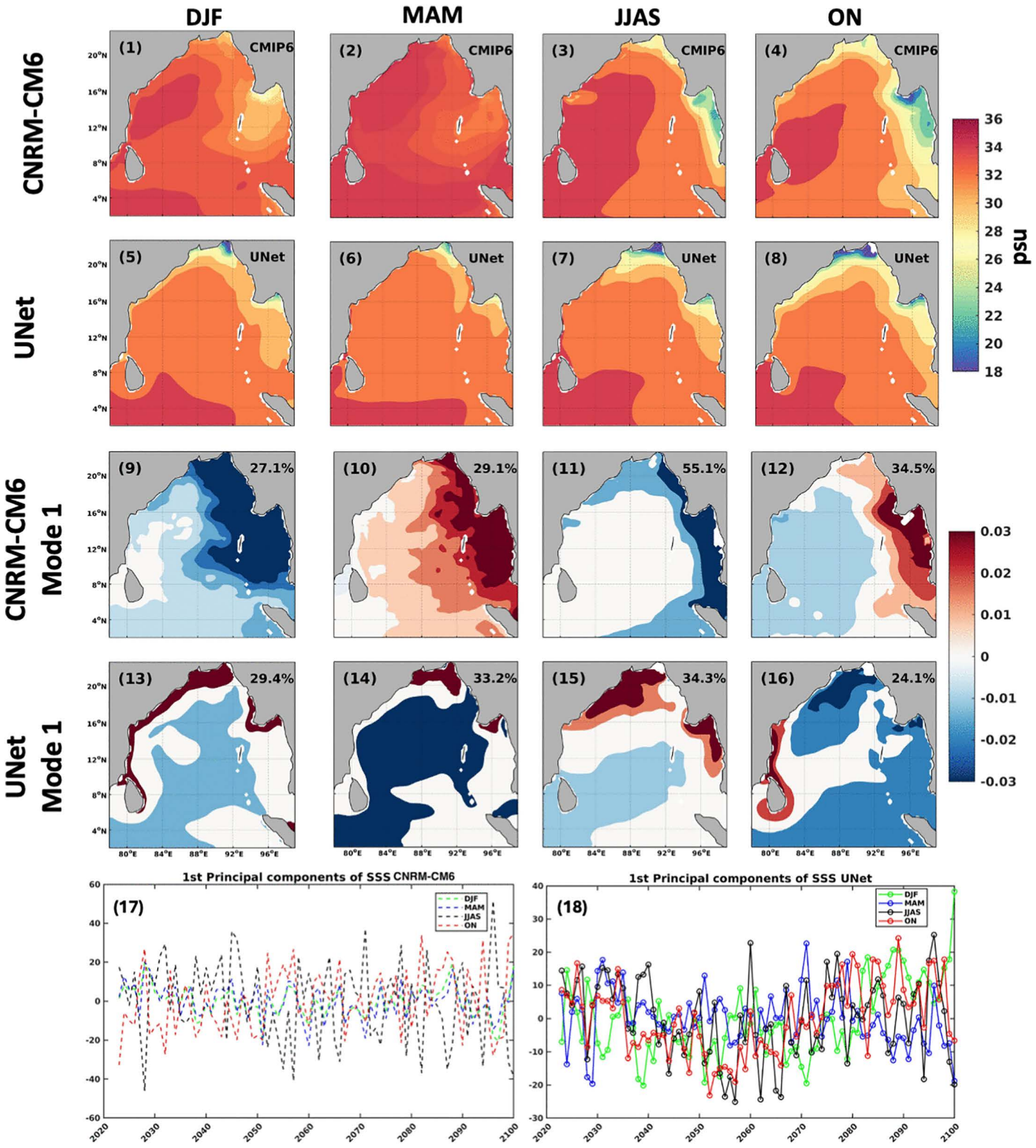

Fig 4. Evaluation of seasonal SSS in test period. Seasonal mean sea surface salinity (SSS) in the Bay of Bengal during test period 2021-2023, comparing **(1)** uncorrected CNRM-CM6 model output (CNRM-CM6), **(2)** ORAS5 reanalysis, **(3)** UNet-corrected salinity (UNet), and **(4)** EDCDF corrected salinity (EDCDF) in DJF, MAM, JJAS, ON seasons. Coastline is extracted from NOAA's ETOPO [13].

https://doi.org/10.1371/journal.pclm.0000749.g004

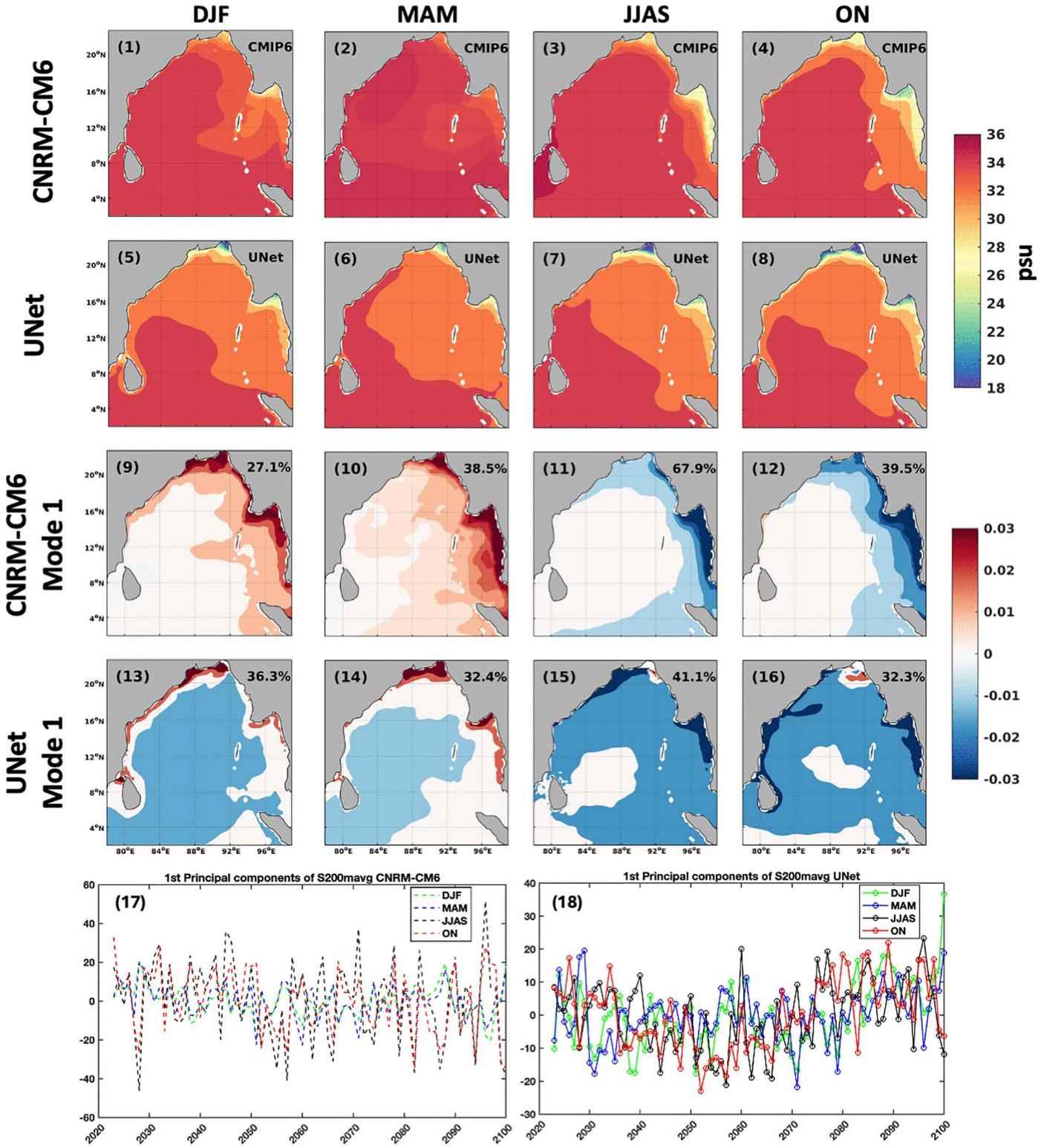

Fig 5. Evaluation of seasonal S200mavg in test period. Seasonal mean 200 m depth-averaged salinity (S200mavg) in the Bay of Bengal during test period 2021-2023, comparing **(1)** uncorrected CNRM-CM6 model output (CNRM-CM6), **(2)** ORAS5 reanalysis, **(3).** UNet-corrected salinity (UNet), and **(4)** EDCDF corrected salinity (EDCDF) in DJF, MAM, JJAS, ON seasons. Coastline is extracted from NOAA's ETOPO [13].

https://doi.org/10.1371/journal.pclm.0000749.g005

salinity for both surface and depth-averaged salinities throughout the basin. In contrast, the UNet corrections show good agreement with ORAS5, accurately capturing the patterns influenced by the southward-flowing EICC.

During the pre-monsoon season, ORAS5 exhibits a basin-wide increase in salinity, with southern regions reaching 32–34 psu for both SSS (Fig 4(b) (MAM)) and S200mavg (Fig 5(b) (MAM)). The uncorrected CNRM-CM6 continues to show a pronounced positive bias across the basin for both variables. However, our UNet corrections effectively reduce this bias and reproduce spatial patterns that are closer to the ORAS5 reanalysis.

The monsoon season is marked by intense SSS freshening in the northern bay (16–20 psu) due to precipitation and river discharge, while the southern regions maintain higher salinity (Fig 4(c) (JJAS)). This freshening is also reflected, though more moderately in the S200mavg fields (26–30 psu; Fig 5(c) (JJAS)). The uncorrected CNRM-CM6 does not capture this freshening in both salinity fields. Our UNet corrected salinity projections are more closely aligned with ORAS5, successfully reproducing the freshening and SMC feature in both surface salinity and top 200 m depth-averaged salinity, a critical improvement over both the uncorrected CNRM-CM6 and the EDCDF-corrected projections.

The post-monsoon period shows a gradual recovery of SSS (Fig 4(d)(ON)) and S200mavg (Fig 5(d)(ON)). During this season, UNet continues to excel in identifying these transitional patterns. The salinity fields corrected by UNet exhibit a closer alignment with ORAS5, effectively reproducing the freshening features in both surface and depth-averaged salinity. In general, UNet outperforms in providing more consistent and accurate corrections. Performance metrics indicate that our UNet based on convolutional neural operators is a reliable tool for climate model salinity bias correction in the Bay of Bengal region. For further insights, we examine the monthly projections (instead of the seasonal average) in the test year 2022 in Figures D-E in S1 Text.

3.3 Mean and interannual variability of salinity projections

Fig 6 presents the mean, the first mode of variability (Mode 1), and the time series of the first principal component (PC1) for the years 2024–2100, analyzing both the uncorrected CNRM-CM6 data and our UNet corrected surface salinity (Fig 6) as well as the 200-m depth-averaged salinity projections (Fig 7). In this section, we discuss the results for SSP2. Similar analyses for SSP1-2.6, SSP3-7.0, and SSP5-8.5 are shown in the Figure F-K in S1 Text.

The Bay of Bengal exhibits distinct seasonal salinity patterns for surface and depth-averaged salinity over the top 200 m, with notable features evident after UNet correction.

During the winter season (DJF), the uncorrected CNRM-CM6 surface salinity projections (Fig 6(1)) show high salinity concentrations (32.5-34 psu) in the western and southern regions, while the northern and eastern coastal areas show lower salinity (30-31.5 psu). The UNet-corrected surface salinity projection presents a salinity distribution with moderate values (31–32 psu) throughout most of the bay, except for a distinct high-salinity zone (> 33.5 psu) along the southern boundary (Fig 6(5)). For the top 200 m depth-averaged salinity during DJF, the uncorrected CNRM-CM6 projections show high salinity values (33–34 psu) dominating most of the bay, with particularly uniform conditions in the western and southern regions (Fig 6(1)). The UNet correction shows a distinct spatial pattern with moderate salinity throughout the northern and central bays and higher values in the southwestern and southern regions (Fig 7(5)). During this season, the first mode of SSS explains 27.1% of the variance in uncorrected CNRM-CM6 and 29.4% of the variance in the UNet-corrected projections. UNet-corrected mode 1 shows high variability along the northern and western coastal regions, whereas the uncorrected mode 1 shows high variability along the eastern coast. The first mode of S200mavg explains 27.1% of the variance in uncorrected CNRM-CM6 projections and 36.3% in UNet-corrected projections. Here, the correction maintains the positive variability of mode 1 along the northern and coastal boundaries, while introducing a more coherent pattern with negative variability across the central bay.

In uncorrected surface salinity projections, the pre-monsoon (MAM) period displays the highest mean salinity values across all seasons, with extensive areas exceeding 33.5 psu in western and central regions (Fig 6(2)). In the UNet correction, this pattern is changed and shows predominantly moderate values throughout the bay (Fig 6(6)). Similarly, the

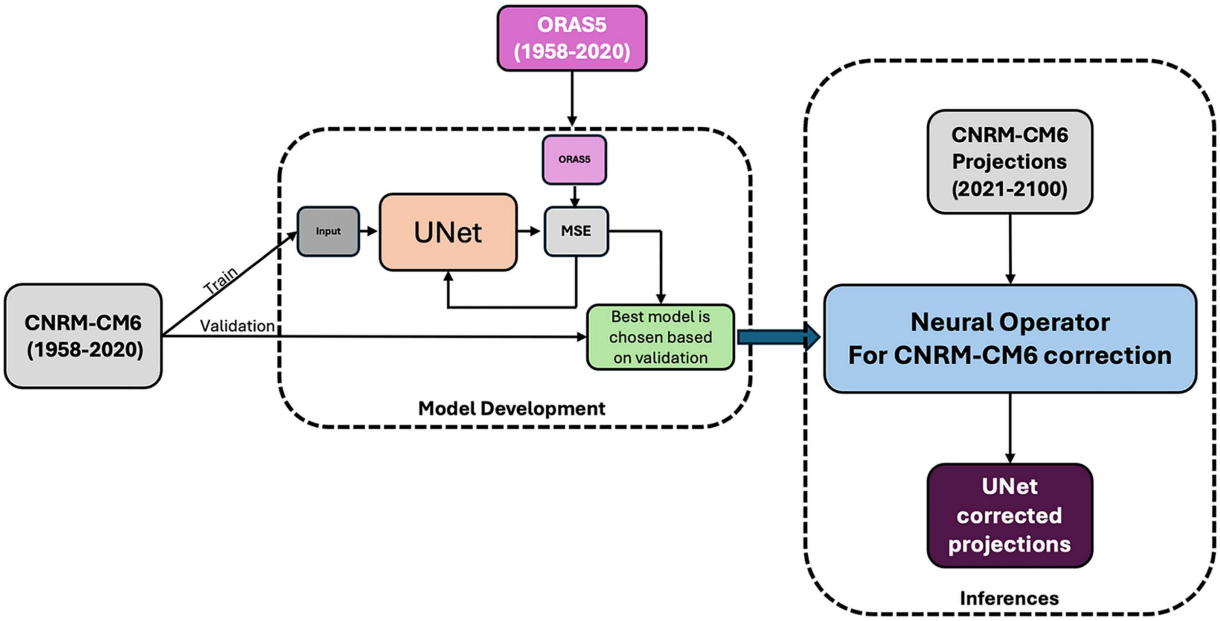

Fig 6. Seasonal SSS temporal evolution from 2023 to 2100. Seasonal mean SSS over the Bay of Bengal comparing uncorrected CNRM-CM6 (1-4) and UNet-corrected. (5–8) projections across DJF (winter), MAM (premonsoon), JJAS (monsoon), and ON (postmonsoon) seasons. Primary EOF modes (Mode 1) of uncorrected CNRM-CM6 (9–12), and UNet-corrected projections (13–16). First Principal Component (PC1) time series for seasonal uncorrected CNRM-CM6 SSS (17) and UNet corrected (18) SSS. Coastline is extracted from NOAA's ETOPO [13].

https://doi.org/10.1371/journal.pclm.0000749.g006

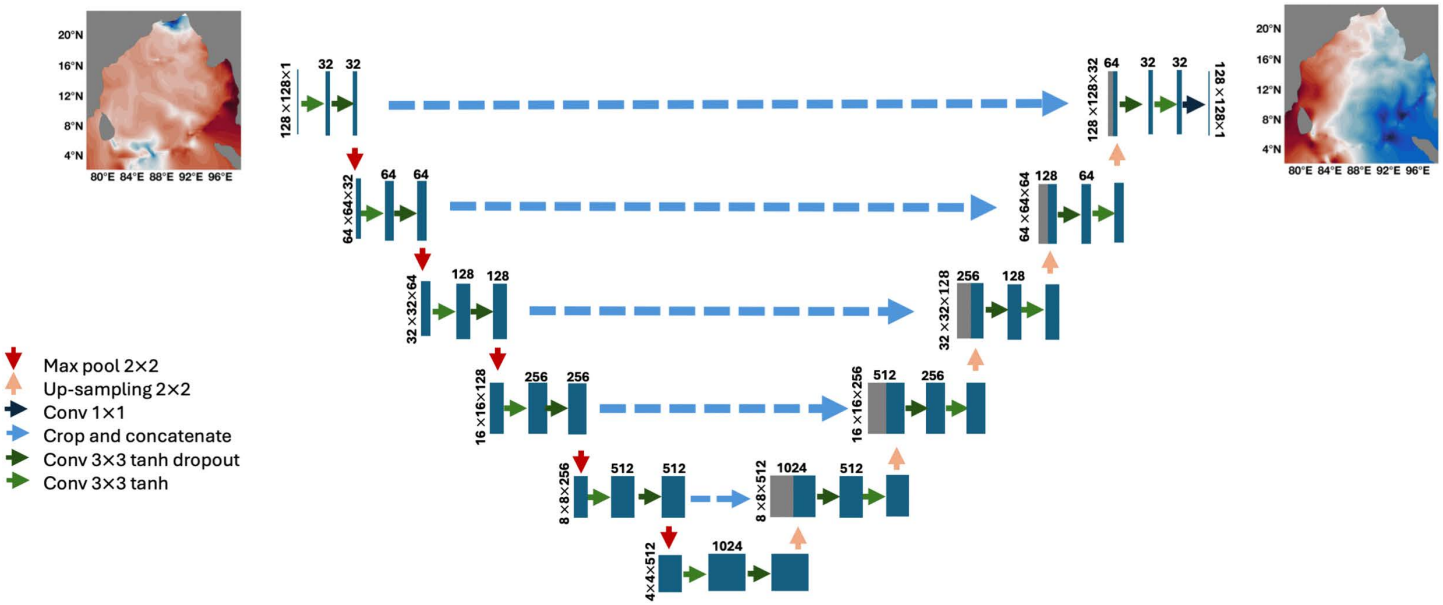

Fig 7. Seasonal S200mavg temporal evolution from 2023 to 2100. Seasonal mean S200mavg over the Bay of Bengal comparing uncorrected CNRM-CM6 (1-4) and UNet-corrected (5-8) projections across DJF (winter), MAM (premonsoon), JJAS (monsoon), and ON (postmonsoon) seasons. Primary EOF modes (Mode 1) of uncorrected CNRM-CM6 (9-12), and UNet-corrected projections (13-16). First Principal Component (PC1) time series for seasonal uncorrected CNRM-CM6 S200mavg (17) and UNet corrected (18) S200mavg. Coastline is extracted from NOAA's ETOPO [13].

https://doi.org/10.1371/journal.pclm.0000749.g007

top 200 m depth-averaged salinity in uncorrected projections exhibits the most intense salinity values with large areas exceeding 34 psu and the highest concentrations appearing in the northwestern and southern regions (Fig 7(2)). However, the UNet correction shows a salinity distribution with moderate values across the northern bay and high salinity regions along the western and southern boundaries (Fig 7(6)). During this season, the first mode of SSS explains 29.1% of the variance in uncorrected CNRM-CM6 and 33.2% of the variance in the UNet-corrected projections. UNet-corrected mode 1 shows high variability in the southwestern and central bay; meanwhile, the uncorrected mode 1 shows high variability in most of the bay. The first mode of S200mavg explains 38.5% of the variance in the uncorrected CNRM-CM6 projections and 32.4% in UNet-corrected projections. The UNet-corrected mode 1 shows significant changes, with high variability in the northern region, and introduces negative variability in the southern regions.

During the monsoon (JJAS), uncorrected surface salinity projections overestimate the persistence of high-salinity waters in western regions despite the freshening influence due to the freshwater influx from river runoff, precipitation, and seasonal currents like SMC (Fig 6(3)). The UNet-corrected surface salinity projections present a monsoon salinity structure with moderate salinity throughout most of the bay and an influx of high salinity water into the bay by SMC (Fig 6(7)). For the top 200 m depth-averaged salinity during the monsoon season, the uncorrected projections continue to show high salinity in most of the bay despite the seasonal freshening influence (Fig 7(3)). The UNet correction shows moderate salinity in the northern and eastern regions and high salinity restricted to the southwest region, showing the characteristics of the SMC and the freshening event in the region (Fig 7(7)). During this season, the first mode of SSS explains 55.1% of the variance in uncorrected CNRM-CM6 projections and 34.3% of the variance in the UNet-corrected projections. The UNet correction shows positive variability along the northern and northeast coasts and negative variability in the southern region along the SMC, which is absent in the uncorrected CNRM-CM6

projections. The first mode of S200mavg explains 67.9% of the variance in the uncorrected CNRM-CM6 projections, but only 41.1% of the variance in the UNet-corrected projections. Here, the UNet-corrected mode 1 maintains the negative variability patterns while introducing a pattern with zero variability in the south central bay. This pattern reveals the influence of the SMC on salinity variability in the Bay of Bengal during the monsoon season. The decrease in variance explained by the primary mode shows that UNet-corrected projections require more modes to represent all features. In addition, the influx of high salinity water from the Arabian Sea by the SMC is now revealed as a primary structure in the first mode of variability, which is absent in the uncorrected CNRM-CM6 projections. In fact, we can see zero variability in most of the bay in uncorrected CNRM-CM6 projections and negative variability near the river influx.

The mean surface salinity of the post-monsoon (ON) season shows a distinctive pattern in uncorrected projections with high salinity around the island of Sri Lanka (Fig 6(4)). The UNet correction shows moderate salinity throughout the bay, with high-salinity water from the southwestern region flowing into the bay, and freshening in the northern bay due to river influx (Fig 6(8)). The top 200 m depth-averaged salinity during the post-monsoon season shows persistent high salinity throughout most of the bay in uncorrected projections, with only slight northeastern freshening during the post-monsoon river influx (Fig 7(4)). The UNet-corrected projections during the post-monsoon present moderate salinity throughout the northern and central regions and a well-defined high salinity region along the southwestern and southern boundaries (Fig 7(8)). During this season, the first mode (Mode 1) of SSS explains 34.5% of the variance in the uncorrected CNRM-CM6 projections, but 24.1% of the variance in the UNet-corrected projections. Here, the UNet-corrected mode 1 shows a distinct pattern of negative variability in most of the bay while introducing positive variability along parts of the coastal boundary. The uncorrected CNRM-CM6 mode 1 shows high variability in the eastern boundary region and zero variability in most of the Bay. The first mode (Mode 1) of S200mavg explains 39.5% of the variance in uncorrected CNRM-CM6 projections and 32.3% in UNet-corrected projections. The UNet-corrected mode 1 shows high variability in the northern and coastal regions and close to zero variability only in the central and southeastern Bay of Bengal. The PC1 time series does not show notable features or differences between the uncorrected and UNet-corrected CNRM-CM6 projections. The implications of these differences are discussed in Section 4.

4 Discussion

Our results show that for the test period (2021–2024), the RMSE when using our UNet-based bias correction method is 0.5 psu for the SSS and 0.25 psu for S200mavg, which is 40% lower compared to the correction by the EDCDF method, the classical statistical bias correction method. The UNet corrected salinity projection allows us to better understand the future salinity scenario in the Bay of Bengal as follows.

Salinity is essential for the development of mangrove ecosystems, promoting their growth when present at moderate levels, but leading to degradation when concentrations are too high [44–46]. The northern and north-western coasts of the Bay of Bengal are crucial mangrove regions. Documented evidence suggests that the lower salinity in these areas is conducive to mangrove growth [47], and salinity variability is also crucial to mangrove health [48]. The UNet-corrected SSS projections indicate that the salinity levels in these regions are lower than the uncorrected projections (Fig 6). However, the spatial pattern of the first mode indicates a higher variability in these areas for the UNet-corrected projection than in the uncorrected CNRM-CM6. Thus, unlike what is expected from uncorrected projections, salinity variability may affect on mangrove health affecting the coastal ecosystem.

The East India Coastal Current (EICC) has been identified as a major mechanism for freshwater export from the Bay of Bengal to the Indian Ocean, primarily in the post-monsoon (ON) and winter (DJF) seasons [5]. Surface salinity has been identified to affect the thickness of the barrier layer [9,49,50] and its intraseasonal variability [51]. The intrusion of freshwater observed from the northern to eastern parts of the bay has been shown to lead to a thicker barrier layer during the monsoon season [49]. The UNet-corrected SSS projections show a lower mean salinity and higher variability along the eastern coast of India during the postmonsoon (ON) and winter season (DJF) than the uncorrected CNRM-CM6 projections (Fig 6). Thus, based on the above studies, we anticipate the significant changes in the thickness of the barrier layer in the future and its intraseasonal variability [52].

The impact of these projected changes has potential implications for the monsoon and ocean productivity. The deepening of the Mixed Layer Depth (MLD) and the variability of the barrier layer are known to influence intraseasonal oscillations during the monsoon in the BoB [10,49,53–55]. Variations in the depth of the mixed layer could also alter the availability of nutrients in the upper ocean, affecting the primary productivity of the region [56]. In the southern Bay of Bengal, the inflow of high-salinity water from the Arabian Sea during the monsoon season (JJAS) is a key feature attributed to the SMC [50,57]. This current affects the thickness of the barrier layer [52]. The uncorrected CNRM-CM6 mean, and the first mode lack SMC, while the first mode of the UNet-corrected surface and top 200 m averaged salinity exhibits the characteristic signature of SMC (Fig 6).

UNet-corrected projections of S200mavg reveal a detailed structure of the SMC during the monsoon season in the Bay of Bengal (Fig 6). The salinity stratification induced by the SMC plays a pivotal role in modulating regional CO_2 dynamics [58]. In addition, the dynamics of the southwest monsoon induce a phytoplankton bloom in the southwest of the Bay of Bengal [59]. The southern Bay of Bengal has been identified as a CO_2 hotspot where the SMC influences carbon fluxes through multiple mechanisms [60]. In addition, SMC-induced salinity gradients affect stratification patterns that control vertical mixing, nutrient delivery, and biological production [61]. The SMC has been shown to influence salinity in the Andaman Sea [11] with implications for the biology of that region. The uncorrected S200mavg CNRM-CM6 projections do not contain the SMC feature (Fig 6). Therefore, it cannot be used to understand the impact of climate change on SMC and other seasonal currents in the Bay of Bengal. In contrast, the UNet-corrected projections contain the SMC feature. The corrected top 200 m depth averaged salinity projections imply that the variability of the SMC could alter with future climate scenarios, potentially greatly impacting the ecosystem of the Bay of Bengal (Fig 6).

5 Conclusion

Motivated by a lack of reliable salinity projections, we developed a deep neural operator for bias correction of the CNRM-CM6 salinity projections in the Bay of Bengal. This model was trained using climatology-removed CMIP6 as input

and the ORAS5 reanalysis product as output for the period in which both fields are available. The trained model corrects the CNRM-CM6 projections for 2024–2100. For the test period (2021–2024), the RMSE when using our correction method is 0.5 for the SSS and 0.25 for the top 200 m depth averaged salinity, which is 40% lower RMSE compared to the correction by the EDCDF method. Using UNet corrected future projections, the seasonal variability (EOF analysis) of SSS and the top 200 m depth averaged salinity in the Bay of Bengal is analyzed. In general, the corrected projections indicate that the reduction in salinity in the northern bay affects the health of mangroves. The significant variability in the UNet corrected salinity in the Bay of Beng al may affect the barrier layer. The UNet-corrected projections capture key features such as the SMC and EICC, and their variability could alter with future climate scenarios, potentially greatly impacting the Bay of Bengal ecosystem. To bolster the bias correction model's robustness, future work could investigate ensemble methods, transfer learning between climate models, and the integration of diverse GCM inputs directly into the training phase.

Supporting information

S1 Text. Table A in S1 Text. Data Sources. Summary of the climate datasets, time frames, and spatial/temporal resolutions used in the study. **Table B in S1 Text. SSS Variance Analysis.** Percentage of variance explained by the primary mode of variability (Mode 1) for SSS across seasons and SSP scenarios. **Table C in S1 Text. S200mavg Variance Analysis.** Percentage of variance explained by the primary mode of variability (Mode 1) for S200mavg across seasons and SSP scenarios. **Figure A in S1 Text. Training and Validation Loss.** Convergence curves for the UNet model for both Sea Surface Salinity (SSS) and top 200m depth-averaged salinity (S200mavg). **Figure B in S1 Text. Taylor Diagram: Model Comparison.** Statistical comparison of uncorrected CNRM-CM6, EDCDF-corrected, and UNet-corrected outputs against ORAS5 reanalysis for SSS and S200mavg across SSP scenarios during the test period. **Figure C in S1 Text. Pixel-wise Correlation Analysis.** Temporally averaged correlation coefficients between ORAS5 and the three datasets (raw CNRM-CM6, EDCDF, and UNet) for SSS and S200mavg during the test period. **Figure D in S1 Text. Monthly SSS Spatial Distribution.** Detailed monthly spatial maps for Sea Surface Salinity in the Bay of Bengal for the year 2022. **Figure E in S1 Text. Monthly S200mavg Spatial Distribution.** Detailed monthly spatial maps for the top 200m depth-averaged salinity in the Bay of Bengal for the year 2022. **Figure F in S1 Text. SSP1-2.6 SSS Scenario Analysis.** Seasonal mean SSS temporal evolution (2023–2100) and primary EOF modes under the SSP1-2.6 pathway. **Figure G in S1 Text. SSP3-7.0 SSS Scenario Analysis.** Seasonal mean SSS temporal evolution (2023–2100) and primary EOF modes under the SSP3-7.0 pathway. **Figure H in S1 Text. SSP5-8.5 SSS Scenario Analysis.** Seasonal mean SSS temporal evolution (2023–2100) and primary EOF modes under the SSP5-8.5 pathway. **Figure I in S1 Text. Seasonal S200mavg (SSP1-2.6).** Seasonal mean and primary EOF modes for top 200m depth-averaged salinity under the SSP1-2.6 pathway. **Figure J in S1 Text. Seasonal S200mavg (SSP3-7.0).** Seasonal mean and primary EOF modes for top 200m depth-averaged salinity under the SSP3-7.0 pathway. **Figure K in S1 Text. Seasonal S200mavg (SSP5-8.5).** Seasonal mean and primary EOF modes for top 200m depth-averaged salinity under the SSP5-8.5 pathway.
(DOCX)

Author contributions

Conceptualization: Abhishek Pasula, Deepak N. Subramani.

Formal analysis: Abhishek Pasula.

Investigation: Abhishek Pasula.

Methodology: Deepak N. Subramani.

Software: Abhishek Pasula.

Supervision: Deepak N. Subramani.

Visualization: Abhishek Pasula.

Writing – original draft: Abhishek Pasula, Deepak N. Subramani.

Writing – review & editing: Deepak N. Subramani.

References

1. Hartmann J, West AJ, Renforth P, Köhler P, De La Rocha CL, Wolf-Gladrow DA, et al. Enhanced chemical weathering as a geoengineering strategy to reduce atmospheric carbon dioxide, supply nutrients, and mitigate ocean acidification. Reviews of Geophysics. 2013;51(2):113–49. https://doi.org/10.1002/rog.20004
2. Durack PJ, Wijffels SE. Fifty-Year Trends in Global Ocean Salinities and Their Relationship to Broad-Scale Warming. Journal of Climate. 2010;23(16):4342–62. https://doi.org/10.1175/2010jcli3377.1
3. Durack PJ, Wijffels SE, Matear RJ. Ocean salinities reveal strong global water cycle intensification during 1950 to 2000. Science. 2012;336(6080):455–8. https://doi.org/10.1126/science.1212222 PMID: 22539717
4. Webster PJ. The role of hydrological processes in ocean-atmosphere interactions. Reviews of Geophysics. 1994;32(4):427–76. https://doi.org/10.1029/94rg01873
5. Shetye SR, Gouveia AD, Shankar D, Shenoi SSC, Vinayachandran PN, Sundar D, et al. Hydrography and circulation in the western Bay of Bengal during the northeast monsoon. J Geophys Res. 1996;101(C6):14011–25. https://doi.org/10.1029/95jc03307
6. Vinayachandran PN, Kurian J. Hydrographic observations and model simulation of the Bay of Bengal freshwater plume. Deep Sea Research Part I: Oceanographic Research Papers. 2007;54(4):471–86. https://doi.org/10.1016/j.dsr.2007.01.007
7. Vinayachandran P, Shetye SR, Sengupta D, Gadgil S. Forcing mechanisms of the Bay of Bengal. Curr Sci. 1996;70(10):753–63. https://www.jstor.org/stable/24048731
8. McCreary JP Jr, Kundu PK, Molinari RL. A numerical investigation of dynamics, thermodynamics and mixed-layer processes in the Indian Ocean. Progress in Oceanography. 1993;31(3):181–244. https://doi.org/10.1016/0079-6611(93)90002-u
9. Shankar D, Vinayachandran PN, Unnikrishnan AS. The monsoon currents in the north Indian Ocean. Progress in Oceanography. 2002;52(1):63–120. https://doi.org/10.1016/s0079-6611(02)00024-1
10. Webber BGM, Matthews AJ, Vinayachandran PN, Neema CP, Sanchez-Franks A, Vijith V, et al. The Dynamics of the Southwest Monsoon Current in 2016 from High-Resolution In Situ Observations and Models. Journal of Physical Oceanography. 2018;48(10):2259–82. https://doi.org/10.1175/jpo-d-17-0215.1
11. Pasula A, Subramani DN. Cause and impact of Andaman Sea's salinity variability: A modeling study. Deep Sea Research Part II: Topical Studies in Oceanography. 2023;209:105291. https://doi.org/10.1016/j.dsr2.2023.105291
12. Du Y, Zhang Y, Shi J. Relationship between sea surface salinity and ocean circulation and climate change. Sci China Earth Sci. 2019;62(5):771–82. https://doi.org/10.1007/s11430-018-9276-6
13. NOAA. 2-minute gridded global relief data (etopo2) v2. 414. Natl Geophys Data Center, NOAA Natl Centers Env Inf. 2006. https://doi.org/10.7289/V5J1012Q
14. Reichstein M, Camps-Valls G, Stevens B, Jung M, Denzler J, Carvalhais N, et al. Deep learning and process understanding for data-driven Earth system science. Nature. 2019;566(7743):195–204. https://doi.org/10.1038/s41586-019-0912-1 PMID: 30760912
15. Gruber N. Warming up, turning sour, losing breath: ocean biogeochemistry under global change. Philos Trans A Math Phys Eng Sci. 2011;369(1943):1980–96. https://doi.org/10.1098/rsta.2011.0003 PMID: 21502171
16. Piani C, Weedon GP, Best M, Gomes SM, Viterbo P, Hagemann S, et al. Statistical bias correction of global simulated daily precipitation and temperature for the application of hydrological models. Journal of Hydrology. 2010;395(3–4):199–215. https://doi.org/10.1016/j.jhydrol.2010.10.024
17. Piani C, Haerter JO. Two dimensional bias correction of temperature and precipitation copulas in climate models. Geophysical Research Letters. 2012;39(20). https://doi.org/10.1029/2012gl053839
18. Cannon AJ, Sobie SR, Murdock TQ. Bias Correction of GCM Precipitation by Quantile Mapping: How Well Do Methods Preserve Changes in Quantiles and Extremes?. Journal of Climate. 2015;28(17):6938–59. https://doi.org/10.1175/jcli-d-14-00754.1
19. Maraun D. Bias Correcting Climate Change Simulations - a Critical Review. Curr Clim Change Rep. 2016;2(4):211–20. https://doi.org/10.1007/s40641-016-0050-x
20. Graham LP, Andréasson J, Carlsson B. Assessing climate change impacts on hydrology from an ensemble of regional climate models, model scales and linking methods – a case study on the Lule River basin. Climatic Change. 2007;81(S1):293–307. https://doi.org/10.1007/s10584-006-9215-2
21. Sennikovs J, Bethers U. Statistical downscaling method of regional climate model results for hydrological modelling. In: Proceedings of the 18th World IMacS/MODSIM congress, 2009. 3962–8. https://mssanz.org.au/modsim09/
22. Li H, Sheffield J, Wood EF. Bias correction of monthly precipitation and temperature fields from Intergovernmental Panel on Climate Change AR4 models using equidistant quantile matching. J Geophys Res. 2010;115(D10). https://doi.org/10.1029/2009jd012882

23. Cannon AJ. Multivariate Bias Correction of Climate Model Output: Matching Marginal Distributions and Intervariable Dependence Structure. Journal of Climate. 2016;29(19):7045–64. https://doi.org/10.1175/jcli-d-15-0679.1
24. Mehrotra R, Sharma A. A Multivariate Quantile-Matching Bias Correction Approach with Auto- and Cross-Dependence across Multiple Time Scales: Implications for Downscaling. Journal of Climate. 2016;29(10):3519–39. https://doi.org/10.1175/jcli-d-15-0356.1
25. Ahijevych D, Pinto JO, Williams JK, Steiner M. Probabilistic Forecasts of Mesoscale Convective System Initiation Using the Random Forest Data Mining Technique. Weather and Forecasting. 2016;31(2):581–99. https://doi.org/10.1175/waf-d-15-0113.1
26. Boukabara S-A, Krasnopolsky V, Penny SG, Stewart JQ, McGovern A, Hall D, et al. Outlook for Exploiting Artificial Intelligence in the Earth and Environmental Sciences. Bulletin of the American Meteorological Society. 2021;102(5):E1016–32. https://doi.org/10.1175/bams-d-20-0031.1
27. Labe ZM, Delworth TL, Johnson NC, Cooke WF. Exploring a data-driven approach to identify regions of change associated with future climate scenarios. Journal of Geophysical Research: Machine Learning and Computation. 2024;1(4):e2024JH000327. https://doi.org/10.1029/2024JH000327
28. Ban~o-Medina J, Iturbide M, Fernández J, Gutiérrez JM. Transferability and explainability of deep learning emulators for regional climate model projections. N/A. 2023. https://doi.org/N/A
29. Wang F, Tian D. On deep learning-based bias correction and downscaling of multiple climate models simulations. Clim Dyn. 2022;59(11–12):3451–68. https://doi.org/10.1007/s00382-022-06277-2
30. Fulton DJ, Clarke BJ, Hegerl GC. Bias Correcting Climate Model Simulations Using Unpaired Image-to-Image Translation Networks. Artificial Intelligence for the Earth Systems. 2023;2(2). https://doi.org/10.1175/aies-d-22-0031.1
31. Zhang S, Li X. Future projections of offshore wind energy resources in China using CMIP6 simulations and a deep learning-based downscaling method. Energy. 2021;217:119321. https://doi.org/10.1016/j.energy.2020.119321
32. Dutta D, Bhattacharjya RK. A statistical bias correction technique for global climate model predicted near-surface temperature in India using the generalized regression neural network. Journal of Water and Climate Change. 2022;13(2):854–71. https://doi.org/10.2166/wcc.2022.214
33. Sharma SCM, Kumar B, Mitra A, Saha SK. Deep learning-based bias correction of ISMR simulated by GCM. Atmospheric Research. 2024;309:107589. https://doi.org/10.1016/j.atmosres.2024.107589
34. Pasula A, Subramani DN. Global climate model bias correction using deep learning. Mach Learn: Earth. 2025;1(1):015001. https://doi.org/10.1088/3049-4753/ade9c3
35. Pasula A, Subramani DN. Data driven deep learning for correcting global climate model projections of SST and DSL in the Bay of Bengal. 2025. Available from: https://arxiv.org/abs/2504.20620. arXiv:2504.20620.
36. Pasula A. AbhiPasula/CNRM-CM6-Salinity-Bias-Correction: CNRM-CM6-Salinity-Bias-Correction Zenodo release. Zenodo; 2025. Available from: https://doi.org/10.5281/zenodo.17947447
37. Voldoire A, Saint-Martin D, S´en´esi S, Decharme B, Alias A, Chevallier M. Journal of Advances in Modeling Earth Systems. 2019;11(7):2177–213. https://doi.org/10.1029/2019MS001683
38. Kuhlbrodt T, Voldoire A, Palmer MD, Geoffroy O, Killick RE. Historical Ocean Heat Uptake in Two Pairs of CMIP6 Models: Global and Regional Perspectives. of Journal Climate. 2023;36(7):2183–203. https://doi.org/10.1175/jcli-d-22-0468.1
39. Madec G, Bourdallé-Badie R, Bouttier PA, Bricaud C, Bruciaferri D, Calvert D, et al. NEMO ocean engine. Institut Pierre-Simon Laplace (IPSL). 2017. https://doi.org/10.5281/zenodo.1464816
40. Zuo H, Balmaseda MA, Tietsche S, Mogensen K, Mayer M. The ECMWF operational ensemble reanalysis–analysis system for ocean and sea ice: a description of the system and assessment. Ocean Sci. 2019;15(3):779–808. https://doi.org/10.5194/os-15-779-2019
41. Sachindra D, Huang F, Barton AF, Perera BJ. Statistical downscaling of general circulation model outputs to precipitation. In: Hydrology and Water Resources Symposium 2012, 2012. 595–602. https://doi.org/10.1002/joc.3914
42. Yang X, Wood EF, Sheffield J, Ren L, Zhang M, Wang Y. Bias Correction of Historical and Future Simulations of Precipitation and Temperature for China from CMIP5 Models. Journal of Hydrometeorology. 2018;19(3):609–23. https://doi.org/10.1175/jhm-d-17-0180.1
43. Mondal SK, Tao H, Huang J, Wang Y, Su B, Zhai J, et al. Projected changes in temperature, precipitation and potential evapotranspiration across Indus River Basin at 1.5-3.0 °C warming levels using CMIP6-GCMs. Sci Total Environ. 2021;789:147867. https://doi.org/10.1016/j.scitotenv.2021.147867 PMID: 34052498
44. Paliyavuth C, Clough B, Patanaponpaiboon P. Salt uptake and shoot water relations in mangroves. Aquatic Botany. 2004;78(4):349–60. https://doi.org/10.1016/j.aquabot.2004.01.002
45. Mitra A, Chowdhury R, Sengupta K, Banerjee K. Impact of salinity on mangroves. Journal of Coastal Environment. 2010;1(1):71–82.
46. Dasgupta S, Islam MS, Huq M, Huque Khan Z, Hasib MR. Quantifying the protective capacity of mangroves from storm surges in coastal Bangladesh. PLoS One. 2019;14(3):e0214079. https://doi.org/10.1371/journal.pone.0214079 PMID: 30897133
47. Chaudhuri AB, Choudhury A. Mangroves of the Sundarbans. International Union for Conservation of Nature and Natural Resources (IUCN). 1994.
48. Banerjee K, Gatti RC, Mitra A. Climate change-induced salinity variation impacts on a stenoecious mangrove species in the Indian Sundarbans. Ambio. 2017;46(4):492–9. https://doi.org/10.1007/s13280-016-0839-9 PMID: 27804094
49. Thadathil P, Muraleedharan PM, Rao RR, Somayajulu YK, Reddy GV, Revichandran C. Observed seasonal variability of barrier layer in the Bay of Bengal. J Geophys Res. 2007;112(C2). https://doi.org/10.1029/2006jc003651

50. George JV, Vinayachandran PN, Vijith V, Thushara V, Nayak AA, Pargaonkar SM, et al. Mechanisms of Barrier Layer Formation and Erosion from In Situ Observations in the Bay of Bengal. Journal of Physical Oceanography. 2019;49(5):1183–200. https://doi.org/10.1175/jpo-d-18-0204.1
51. Rao RR, Sivakumar R. Seasonal variability of sea surface salinity and salt budget of the mixed layer of the north Indian Ocean. J Geophys Res. 2003;108(C1). https://doi.org/10.1029/2001jc000907
52. Callaghan AH, Ward B, Vialard J. Influence of surface forcing on near-surface and mixing layer turbulence in the tropical Indian Ocean. Deep Sea Research Part I: Oceanographic Research Papers. 2014;94:107–23. https://doi.org/10.1016/j.dsr.2014.08.009
53. Girishkumar MS, Ravichandran M, McPhaden MJ, Rao RR. Intraseasonal variability in barrier layer thickness in the south central Bay of Bengal. J Geophys Res. 2011;116(C3). https://doi.org/10.1029/2010jc006657
54. Li Y, Han W, Ravichandran M, Wang W, Shinoda T, Lee T. Bay of Bengal Salinity stratification and Indian summer monsoon intraseasonal oscillation: Intraseasonal variability and causes. Journal of Geophysical Research: Oceans. 2017;122(5):4291–311. https://doi.org/10.1002/2017JC012691
55. Li Y, Han W, Wang W, Ravichandran M, Lee T, Shinoda T. Bay of Bengal salinity stratification and Indian summer monsoon intraseasonal oscillation: 2. Impact on SST and convection. JGR Oceans. 2017;122(5):4312–28. https://doi.org/10.1002/2017jc012692
56. Narvekar J, Prasanna Kumar S. Mixed layer variability and chlorophyll a biomass in the Bay of Bengal. Biogeosciences. 2014;11(14):3819–43. https://doi.org/10.5194/bg-11-3819-2014
57. Vinayachandran PN, Masumoto Y, Mikawa T, Yamagata T. Intrusion of the Southwest Monsoon Current into the Bay of Bengal. J Geophys Res. 1999;104(C5):11077–85. https://doi.org/10.1029/1999jc900035
58. Gauns M, Madhupratap M, Ramaiah N, Jyothibabu R, Fernandes V, Paul JT, et al. Comparative accounts of biological productivity characteristics and estimates of carbon fluxes in the Arabian Sea and the Bay of Bengal. Deep Sea Research Part II: Topical Studies in Oceanography. 2005;52(14–15):2003–17. https://doi.org/10.1016/j.dsr2.2005.05.009
59. Muraleedharan K, Jasmine P, Achuthankutty C, Revichandran C, Kumar PD, Anand P. Influence of basin-scale and mesoscale physical processes on biological productivity in the Bay of Bengal during the summer monsoon Progress in oceanography. Prog Oceanogr. 2007;72(4):364–83. https://doi.org/10.1016/j.pocean.2006.09.012
60. Roy R, Vinayachandran PN, Sarkar A, George J, Parida C, Lotliker A, et al. Southern Bay of Bengal: A possible hotspot for CO2 emission during the summer monsoon. Progress in Oceanography. 2021;197:102638. https://doi.org/10.1016/j.pocean.2021.102638
61. Jyothibabu R, Vinayachandran PN, Madhu NV, Robin RS, Karnan C, Jagadeesan L, et al. Phytoplankton size structure in the southern Bay of Bengal modified by the Summer Monsoon Current and associated eddies: Implications on the vertical biogenic flux. Journal of Marine Systems. 2015;143:98–119. https://doi.org/10.1016/j.jmarsys.2014.10.018